Field Emission Properties of Gold Nanoparticle-Decorated ZnO Nanopillars

ARTICLE *in* ACS APPLIED MATERIALS & INTERFACES · NOVEMBER 2012

Impact Factor: 6.72 · DOI: 10.1021/am301848a · Source: PubMed

THE JOURNAL OF PHYSICAL CHEMISTRY C

Article

pubs.acs.org/JPCC

Optoelectronic Properties of Density-Controlled ZnO Nanopillar Arrays

Yuan-Ming Chang,*[,†] Jheng-Ming Huang,[§] Chih-Ming Lin,[∥] Hsin-Yi Lee,[⊥,‡] San-Yuan Chen,[‡] and Jenh-Yih Juang*[,†]

[†]Department of Electrophysics, [‡]Department of Materials Science and Engineering, and [§]Program for Science and Technology of Accelerator Light Source, National Chiao Tung University, Hsinchu 300, Taiwan

[∥]Department of Applied Science, National Hsinchu University of Education, Hsinchu 300, Taiwan

[⊥]National Synchrotron Radiation Research Center, Hsinchu 300, Taiwan

ABSTRACT: An effective method of controlling the density of ZnO nanopillars (ZnO-NPs) by using the self-assembled silver nanoislands as the growth catalyst is demonstrated. We were able to vary the density of the ZnO-NPs to within the range of ~10−30 μm^{-2} by properly manipulating the size distribution of the silver nanoislands partially covering the Si substrates. Continuous silver film can also be used as the catalyst to facilitate the growth of ZnO islands and pillars on Si substrates, albeit with much less control of the resultant density and morphological appearances. The field-emission measurements indicate that the performance of field emission for ZnO-NPs can be improved markedly by reducing the density of the ZnO-NPs. The turn-on field of the low-density ZnO-NPs was as low as 2.39 V/μm with a corresponding current density of 10 $\mu A/cm^2$ and a field enhancement factor (β value) of ~3500. The enhancement of field-emission characteristics is attributed to the much reduced field screen effect by properly controlled density of the ZnO-NPs.

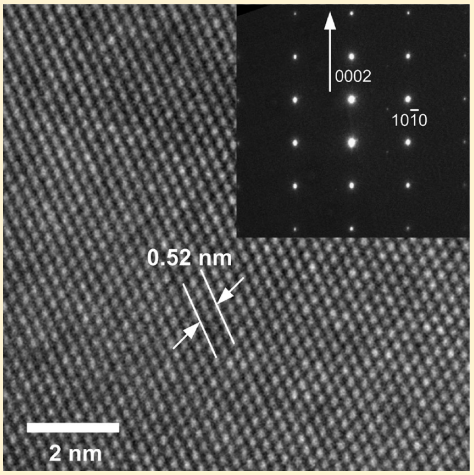

1. INTRODUCTION

One-dimensional (1-D) nanostructures of various semiconductors have attracted tremendous research interest in recent years due to their highly anticipated potential in realizing a wide variety of applications in high-performance micro-to-nanoscale optoelectronic devices.[1−5] Among them, the 1-D ZnO nanostructures, including wires, rods, and pillars, have been considered as potential candidates for electronic field emitters due to their excellent thermal and chemical stabilities.[6,7] Consequently, a plethora of approaches were developed in combination with different catalysts to fabricate 1-D ZnO nanostructures.[8−10] For instance, it has been reported that ZnO nanostructures could be obtained by thermal evaporation without using catalyst.[11] The resultant ZnO nanostructures, however, exhibited a broad photoluminescence (PL) emission peak covering almost the entire visible region, indicating the defective characteristics of the obtained nanostructures. It is generally conceived that density control of ZnO nanopillars (ZnO-NPs) is very important to optimize their field-emission characteristics. Unfortunately, reproducible control of the aspect ratio of individual nanopillar as well as the spacing between them has been a harsh challenge and yet-to-be-resolved technical issue, especially for those prepared by using vapor phase transport method. It appeared that resorting to catalytic growth might be a necessity. Compared with gold, silver (Ag) has received only scant attention as the catalyst for growing ZnO nanostructures. Although Ag is chemically similar to gold, it, nevertheless, does have a lower melting point and is more reactive as compared with gold. For that matter, Ag may be an even more promising candidate to be used as catalyst for growing ZnO nanostructures in a controllable manner, which apparently will play crucial roles in realizing high-performance optoelectronic micronanodevices based on ZnO nanostructures.

In this study, we report an effective method of synthesizing ZnO-NPs array on Si-substrates with controlled density by using self-assembled Ag nanoislands as catalyst. The density of the self-assembled Ag nanoislands was monitored by a single-step sputtering process or direct dry etching subsequently performed. The simplicity of the present fabrication method is thus advantageous in several respects. First, the manufacturing process is very effective because it took only 10 s to obtain the self-assembled Ag nanoislands. Moreover, because the Ag nanoislands are obtained by a single-step sputtering process and no heat treatment is needed to create the nanoislands, it can significantly reduce the energy consumption. More importantly, when the Ag nanoislands are used to catalyze the growth of ZnO-NPs, the density can be readily manipulated, which, in

Received: February 10, 2012
Revised: March 18, 2012
Published: March 20, 2012

dx.doi.org/10.1021/jp301350h | J. Phys. Chem. C 2012, 116, 8332−8337

turn, may have significant implications in field-emission applications.

2. EXPERIMENTAL SECTION

The Ag nanoislands grown on Si substrates were obtained by rf sputtering (Eastern Sharp EPS01) from an Ag target for 10 s with an input power of 150 W in a 25 sccm argon gas atmosphere. Because of the short sputtering time practiced, the resultant size distribution of the obtained Ag nanoislands is rather uneven. When the sputtering time was increased to 5 min, a continuous layer of Ag film was obtained. In either case, the density of the resultant Ag nanoislands on Si substrates can be further modified by subsequent dry etching performed in a metal etcher system. Prior to etching, the chamber was evacuated to a base pressure of $\sim 3 \times 10^{-5}$ Torr while the temperature of the system was kept at 60 °C. After the prepared Ag nanoislands covered Si substrate was loaded, 90 sccm of Cl_2 gas and 10 sccm of N_2 gas were simultaneously introduced. The system was operated with a fixed input power of 1900 W with the etching time being maintained for ~1 min. Si wafers covered with various densities of Ag nanoislands, including the ones covered with an entire layer of Ag film, were then cut into 2×2 cm^2 pieces and used as the substrates for the subsequent growth of ZnO-NPs.

The ZnO-NPs were fabricated via a simple vapor-phase transport process in a horizontal quartz tube furnace. A quartz boat loaded with 0.5 g of Zn powder was placed within the heating zone, which was set at 780 °C. During the heating process, Zn was first evaporated and then transferred by the flowing mixed gas of Ar (500 sccm) and oxygen (30 sccm) to the Ag-coated Si substrates placed about 2 cm downstream from the Zn source for 30 min. The temperature at the position of the Si substrate was about the same as the source temperature. The ZnO-NPs were obtained through the catalyzed reactions between Zn and oxygen.

The morphology of the Ag nanoislands and the obtained ZnO nanostructures was examined by a field-emission scanning electron microscope (FESEM, JEOL JSM-6700F), and the relevant compositions were analyzed with the energy-dispersive X-ray spectroscopy (EDS) attached to the FESEM. High-resolution X-ray diffraction (HRXRD, PANalytical X'Pert Pro Singapore, with Cu Kα; λ = 0.154 nm) was used to determine the phase and crystallographic structure of all samples. The PL measurements were performed down to the lowest temperature of 12 K using a He−Cd laser (325 nm, IK3252R-E, Kimmon) for excitation and a charge-coupled diode (CCD, 80 K, Spec-10, Princeton Instruments) with a monochromator (0.5 m, SP-2558A, Acton) for detection. The effective wavelength resolution of the PL spectrum was better than 0.02 nm. For the field-emission measurements, the samples were loaded into a vacuum chamber (5×10^{-6} Torr). A transparent conductive oxide (indium−tin-oxide) coated with a layer of phosphor (P_{22}) was used to serve as the anode electrode of the vacuum system, and the cathode voltage was applied to all ZnO samples (1×1 cm^2).

3. RESULTS AND DISCUSSION

Figure 1a shows the typical morphology and distribution of the Ag nanoislands obtained with a sputtering time of 10 s. The density of the Ag nanoislands is estimated to be around 4.5×10^9 cm^{-2}. It is evident from the SEM image that, in addition to the isolated islands with smaller sizes, it does appear to have

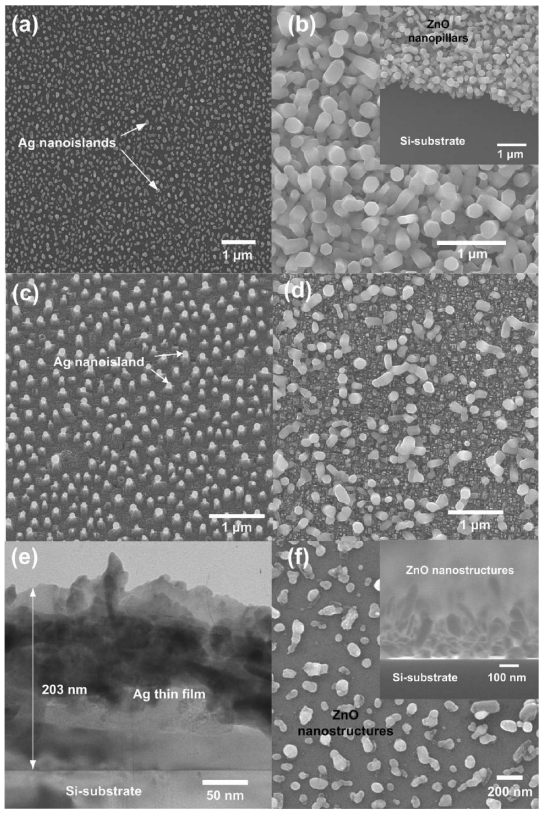

Figure 1. (a) SEM images of Ag nanoislands evenly distributed on Si substrate. (b) SEM image of ZnO-NPs that were grown on panel a, namely, sample A. The inset in panel b shows that the Si substrate is partially covered by ZnO-NPs. (c) SEM image of Ag nanoislands that have been processed dry etching for 1 min. (d) SEM image of ZnO-NPs that were grown on panel c, namely, sample B. (e) Cross-sectional TEM image of continuous Ag film on Si substrate. (f) Top-view SEM image of ZnO-nanostructures that were grown on panel e, namely, sample C, and the inset is the cross-sectional SEM image of panel f.

islands resulted from coalescence of two or more islands already even in this short sputtering time. Both of these characteristics are believed to have resulted from the film growth mechanism inherent to Ag on oxidized Si surfaces.[12,13] Compared with the sputtering and postannealing two-step process used to obtain Ag nanoparticles for catalyzing growth of ZnO nanorods previously reported by Zhang et al.,[14] the present single-step process represents a much more efficient alternative to obtain self-assembled Ag nanoislands. The SEM image displayed in Figure 1b shows the typical morphology of the as-synthesized ZnO-NPs arrays using the distribution of Ag nanoislands shown in Figure 1a as the growth catalyst. Hereafter, this sample will be termed as "sample A", and as is evident from the SEM image, the resultant ZnO-NPs are having a mean radius of ~200 nm with a density of 30 to 35 μm^{-2}. It is noted that the use of growth catalyst, such as Ag nanoislands demonstrated here, is of vital importance for the vapor phase transport growth of ZnO nanostructures. The inset of Figure 1b shows an example of growing ZnO-NPs using Si substrates partially covered by Ag islands fabricated with the same conditions as those for sample A. It is evident that the ZnO-NPs grow only in the area coated with Ag nanoislands, and there is essentially no sign of ZnO growth on the bare Si surface. The density of the resultant ZnO-NPs obtained under

dx.doi.org/10.1021/jp301350h | J. Phys. Chem. C 2012, 116, 8332−8337

these conditions, though appears to be too dense for field-emission purpose (vide infra), nevertheless indicates the effectiveness of using Ag as the catalyst for growing ZnO-NPs.

To modify the density of ZnO-NPs, we have carried out a dry etching process to change the density distribution of the sputtering-derived Ag nanoislands on Si substrates. Figure 1c displays an example of the obtained Ag nanoislands distribution after performing 1 min of dry etching process to that shown in Figure 1a. It is evident that the density of the ZnO-NPs is much lower than that displayed in Figure 1a, and apparent damages on the Si substrate are also visible. The density of the ZnO-NPs synthesized by using these 1 min dry-etching-treated substrates (see Figure 1d) is about 10−15 μm^{-2}, which is much lower than that shown in Figure 1b and may have important implications in terms of enhancing field-emission properties. The samples obtained by this process will be denoted as "sample B" for the subsequent discussions below. For comparison purpose, we also grew ZnO-NPs with substrates covered by a continuous ∼200 nm thick Ag layer (Figure 1e). As displayed in Figure 1f, the morphology of the obtained ZnO nanostructures consists of sparsely distributed ZnO islands and pillars with an average density of 20−25 μm^{-2}. Hereafter, it will be denoted as "sample C". From the side view SEM image shown in the inset of Figure 1f, it is clear that the growth of ZnO on the continuous Ag film was not as uniformly catalyzed as those obtained by using Ag nanoislands described in the previous two cases.

The effectiveness of various catalysts used for growing oxides nanostructures has been extensively investigated and compared.[14−16] Nguyen et al.[15] used 16 different metal catalysts to investigate the correlation between catalyst selection and morphology of tin oxide nanowires grown within a 840−860 °C window with a constant Ar (99.999%) carrier gas flow rate of 450 sccm. It was concluded that the growth density of the nanowires is an inverse function of the melting temperature of the metal catalyst and the catalyst material might have served as the soft template for incorporating the vapor species into the nanowires. Therefore, the primary mechanism of growing 1-D nanostructures is through the vapor−liquid−solid (VLS) mechanism, and the vapor−solid (VS) mechanism alone cannot produce nanowires. On the basis of the characteristics of being physically active and chemically inert, Zhang et al.[14] specifically chose Au, Pt, and Ag as the catalysts to control and investigate the growth mechanism of ZnO nanostructures. It was found that for Au and Pt the VLS mechanism is dominant at the growth temperature of 800 °C. However, at 500 °C, the VS mechanism appeared to be prevailing, even though the Au and Ag nanoparticles remained as liquid owing to the high Zn vapor pressure. Zhao et al.[16] compared the Au/Si, ZnO/Si, and Au/ZnO/Si combinations for growing ZnO nanorods at a growth temperature of 950 °C. They found that the addition of the ZnO buffer layer is essential for growing the vertically aligned ZnO nanorods, primarily due to the effects originated from (002)-oriented ZnO buffer layer, which induced either (111)-oriented Au nanoclusters or direct homoepitaxial nucleation. However, because of the low melting point (∼419 °C) of Zn and ZnO_x ($x < 1$), they concluded that at the growth temperature of 950 °C there is no liquid phase present in the process. Therefore, the nanorod growth is governed primarily by the VS mechanism. It appears that the predominant mechanism of the catalytic growth of oxide nanostructures is much more complicated than previously expected and may strongly depend on the detailed process conditions practiced.

In the present case, because the resultant ZnO-NPs all display the hexagonal facet structure with no trace of residual Ag catalyst remaining at the tips (Figures 1b,d,f), it is suggestive that the VLS mechanism may not be the primary operative mechanism. Figure 2a displays the cross-sectional TEM image

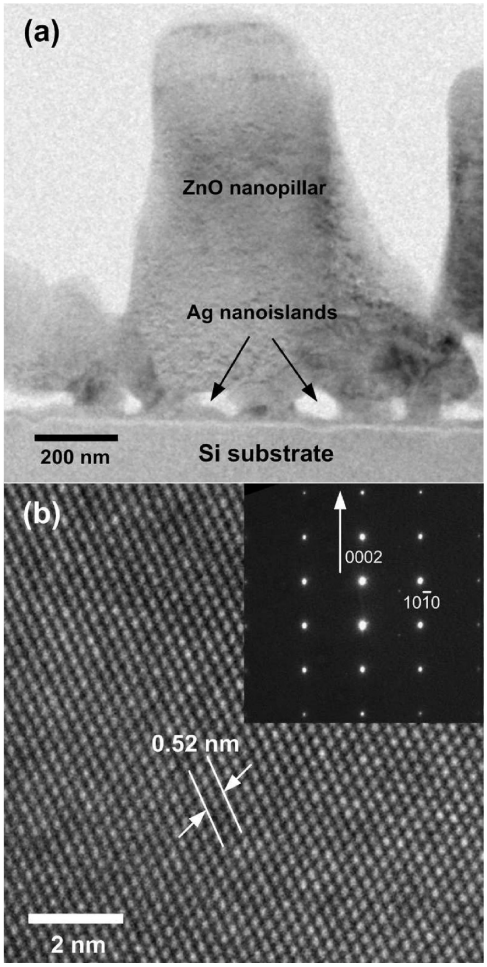

Figure 2. (a) TEM image of individual ZnO-NP and (b) high-resolution TEM image of an individual ZnO-NP. The inset reveals the corresponding selected-area electron diffraction pattern from the nanopillars.

of an individual ZnO-NP taken from sample A. The TEM image clearly indicates that the growth of each individual ZnO-NP was catalyzed by three to four Ag nanoislands. Furthermore, as shown in Figure 2b and the accompanying inset, the HRTEM image and corresponding selective area diffraction evidently display the single-crystalline features of the obtained ZnO-NPs. The lattice spacing between the adjacent lattice planes was ∼0.26 nm, which is consistent with the distance between two (0002) crystal planes in bulk wurtzite-structured ZnO crystal. It is interesting to note that whereas the ZnO-NPs have grown to ∼1 μm high, the size of the catalysts remained essentially unchanged (e.g., by comparing Figure 1a and Figure 2a). This is indicative that in the present case the dominant growth mechanism probably was not the VLS mechanism. Otherwise, one would expect to observe features similar to those described by Hannon et al.[17] in growing Si nanowires on Si substrate with Au nanoparticles as the catalyst. In other words, one should observe the depletion of Ag

dx.doi.org/10.1021/jp301350h | J. Phys. Chem. C 2012, 116, 8332−8337

nanoislands through the growth fronts that would leave some residual metal drop at the tips or eventually terminate the nanopillar growth when the associated metal catalyst was completely consumed. To this respect, it is also surprising to observe that in the present case the individual ZnO-NP is essentially a single crystal, albeit it appeared to simultaneously nucleate on several Ag islands. We note that similar results have been reported by Fan et al.[18] in their study of using patterned Au catalyst to grow large area ZnO-NPs arrays on GaN/Si templates. From their time-sequenced experiments, it was concluded that the whole growth process of the ZnO-NPs was a combination of the VLS and VS mechanisms. In the early stage, the formation of Au−Zn alloys and the subsequent precipitation and oxidation of Zn was responsible for forming the initial (0002)-oriented ZnO nuclei. Then, the VS mechanism took over to control the subsequent anisotropic crystal growth that leads to eventual micrometer-long ZnO-NPs. Within the context of this scenario, because the Ag nanoislands are at temperatures (~780 °C) well above the melting point of Zn (420 °C), the rich unsaturated bonds on the their surfaces could act as nucleation sites for the initial catalytic growth of ZnO-NPs. This may also explain the differences in both the morphologies and densities of the resultant ZnO-NPs displayed in Figure 1. Namely, the smallest Ag nanoislands shown in Figure 1a result in the most efficient catalytic effect and hence the densest ZnO-NPs (Figure 1b) with single-crystalline quality, whereas the continuous Ag film (Figure 1e), owing to the reduced surface activities, can lead only to sparsely distributed ZnO "extrusions" with no distinct crystallographic features (Figure 1f).

To further delineate the structural properties of the ZnO-NPs grown on templates coated with different distributions of catalyst, We carried out X-ray diffraction (XRD) measurements. Figure 3 shows the XRD patterns of the samples A−C,

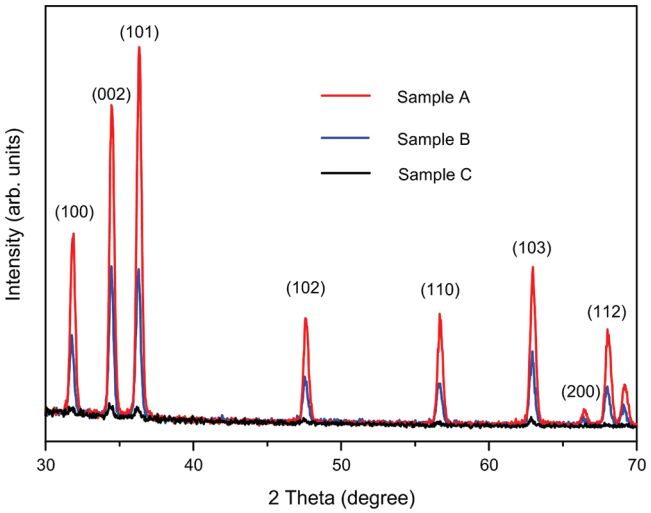

Figure 3. XRD spectra of ZnO samples A−C, respectively.

respectively. It is evident that all diffraction peaks are corresponding to wurzite structure ZnO, indicating the single-phase characteristic of the obtained ZnO-NPs. The fact that virtually all peaks show up in the XRD results might be because the ZnO-NPs are not perfectly aligned normal to the substrate surface. Furthermore, samples A and B apparently are having much better crystalline quality than sample C, albeit the relative intensity between (002) and (101) peaks also indicates that the ZnO-NPs in sample B are more of (0002)-oriented nature. This is also consistent with the fact that in the case of sample B the Ag nanoislands are more isolated (Figure 1c) and the VS growth may take control early to facilitate anisotropic growth.

From the above-mentioned structure examinations by XTEM and XRD, it appears that the ZnO-NPs are of excellent crystalline quality. It is thus interesting to examine further the optical properties of the present ZnO-NPs. Because of many attractive optical properties ubiquitously exhibited in various ZnO nanostructures, the PL properties of ZnO have been the subject of extensive research.[19−23] Figure 4 shows the low-

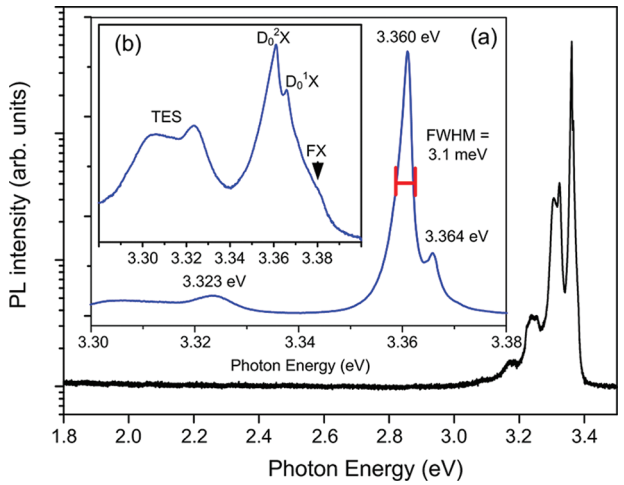

Figure 4. PL spectra (in log scale) obtained for the sample A measured at 12 k. The insets (a) and (b) are the PL characteristic peaks in near-band-edge of sample A.

temperature (12 K) PL spectra for sample A. Notice that the intensity is plotted on the logarithmic scale. We note here that similar results were also obtained for sample B, except for relatively lower PL intensities. The low-temperature PL spectra evidently reveal only the near-band-edge fine excitonic emissions with no discernible emissions in the visible range, indicating that the ZnO-NPs are nearly free of defects. The visible PL emissions at low temperature observed in various ZnO structures have been the subject of extensive research,[24−27] and it is generally conceived that the green-yellow PL emission from ZnO is primarily due to oxygen-related defects.[28,29] Among the ultraviolet (UV) PL peaks, the dominant emission peaks at 12 K were observed at 3.360 to 3.367 eV. The free exciton emission (FX) positioned at 3.380 eV can also been observed, as indicated by the arrow shown in inset (b) of Figure 4. The D_0^2X is the strongest peak with a narrow full width at half-maximum (fwhm) of 3.1 meV (as indicated in inset (a) of Figure 4). The dominance of these donor-bound exciton recombinations differs from that reported by Fonoberov et al.[21] for ZnO nanodots (~4 nm in diameter) and ZnO nanocrystals (~20 nm). In that, the predominant recombination was the acceptor-bound excitons at temperatures below 150 K and was attributed to the large surface-to-volume ratio in both types of nanoparticles. Because the size of the present ZnO-NPs is much larger than that of the above-mentioned nanodots and nanocrystals, it is not surprising to observe significant reduction of the acceptor defects ubiquitously existing near the surface.[21] All of these features indicate that the present ZnO-NPs are of high crystalline quality and only intrinsic optical characteristics are observed.

dx.doi.org/10.1021/jp301350h | J. Phys. Chem. C 2012, 116, 8332−8337

These results are again in good agreement with the evidence displayed in HRTEM (Figure 2b).

There are other more broadened emission peaks lying at lower energies (3.30 to 3.33 eV). These emissions have been identified as originating from the two-electron satellite (TES) recombination line of the neutral donor-bound excitons. The donor final state can be at either the 1s state (D_0^iX line) or the 2s/2p state (TES_i line), during the recombination of an exciton bound to a neutral donor. The energy between the D_0^iX and TES_i is different from the donor energies in the 1s and 2s/2p states. It has been pointed out that the related donor binding energy can be obtained with high precision by determining the position of the TES.[30] In short, the strong intrinsic UV emission displayed in the present PL spectra evidently indicates a low concentration of oxygen vacancies in the Ag nanoislands-catalyzed ZnO-NPs.

To characterize further the electronic properties of these ZnO-NPs, we have also performed the field-emission measurements on these samples. Figure 5 shows the emission current density versus applied electrical field ($J-E$) curves for the three types of ZnO-NPs obtained in this study. The electric field defined here is calculated by dividing the applied voltage with cathode–anode separation, and thus it is representing an average value. The distance between the two electrodes was fixed at 350 μm, which gives rise to steady field emission for the samples measured in this study. The emission current was measured with the applied voltage varying from 0 to 1000 V. It was found that for sample A (open circles in the $J-E$ plots) there was no detectable emission current emission within the entire range of the applied voltage, presumably due to the large field screen effect arisen from the densely packed ZnO-NPs. It has been demonstrated that when the 1-D nanostructures, such as carbon nanotubes, were brought into close proximity the marked screen effect would lead to a sharp decrease in the local field on the tip of the 1-D nanostructures.[31]

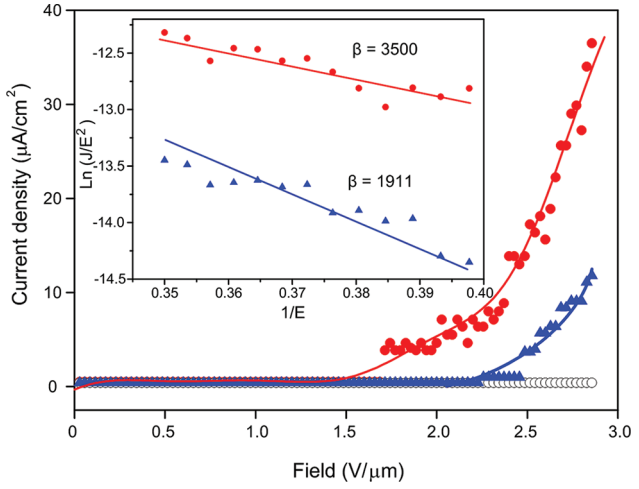

Figure 5. Field-emission $J-E$ curve from the ZnO sample A (open circles), sample B (solid circles), and sample C (solid triangles) at working distance of 350 μm over an effective emitting area of 1 cm^2. The corresponding Fowler–Nordheim plot [$\ln(J/E^2)$ vs $(1/E)$] is shown in the inset.

On the contrary, as can be seen from the $J-E$ plot (solid circles) in Figure 5, for sample B, the turn-on threshold field is ~2.39 V/μm at a current density of 10 μA/cm^2, which is lower than most previously measured ZnO nanostructures.[32−36] Moreover, the emitted current density in this case reaches 36.5 μA/cm^2 at a bias field of 2.86 V/μm. The marked enhancement of field-emission properties for sample B (as compared with sample A) apparently must have arisen from the difference in the density of ZnO-NPs. For sample C, the turn-on threshold field is ~2.82 V/μm at a current density of 10 μA/cm^2 with the maximum emitted current density of 11.8 μA/cm^2 at a bias field of 2.86 V/μm (solid triangles). The moderate decrease in the field-emission performance of sample C could be due to the poor geometric morphology of the obtained ZnO-NPs. (See the inset of Figure 1f.) To understand the emission behavior of the present ZnO-NPs in a more quantitative manner, we analyzed the $J-E$ results by the Fowler-Nordheim (F–N) expression shown below[6]

$$J = \frac{A\beta^2E^2}{\phi}\exp\left(-\frac{B\phi^{3/2}}{\beta E}\right) \quad (1)$$

Here J is the current density (A/m^2), E is the applied field (V/μm), ϕ is the work function (eV), β is the field enhancement factor, and A and B are constants with $A = 1.56 \times 10^{-10}$ (A·eV/V^2) and $B = 6.83 \times 10^3$ (V/μm·eV$^{3/2}$), respectively. The inset in Figure 5 shows the F–N plots for samples B and C. The linear behavior of the ln (J/E^2) versus $1/E$ plot reveals that the field-emission mechanism of the current ZnO-NPs follows the F–N expression well. The field-enhancement factor β was calculated from the slope of the F–N plot[37]

$$\beta = -2.97 \times 10^3 \times \phi^{3/2}/\text{slope} \quad (2)$$

Taking the work function ϕ =5.3 eV for ZnO,[38] the β values are 3500 and 1911 for samples B and C, respectively. The enhancement factor of 3500 is higher than most of the results obtained from various ZnO nanostructures previously reported.[39,40] On the basis of the above results, the present study has evidently demonstrated that by properly controlling the density of the resultant density and morphology of the ZnO-NPs through the manipulations of Ag nanoisland catalyst, excellent field-emission performance with promising industrial applications can be easily attained.

4. CONCLUSIONS

In this study, we have demonstrated the effectiveness of using sputtered Ag nanoislands as the catalyst to grow ZnO-NPs on Si substrates. The growth mechanism, however, is found to be dominated by the VS mechanism, although the VLS might also play a role in the early stage of forming ZnO nuclei. Moreover, the field-emission properties were found to depend strongly on the density of the obtained ZnO-NPs. For samples with appropriate nanopillar densities, the turn-on field of emission is as low as 2.39 V/μm at the corresponding current density of 10 μA/cm^2 with an enhancement factor of 3500.

AUTHOR INFORMATION

Corresponding Author

*Phone: +886-3-5712121, ext. 56116. Fax: +886-3-5725230. E-mail: ymchang7@gmail.com (Y.-M.C.); jyjuang@g2.nctu.edu.tw (J.-Y.J.).

Notes

The authors declare no competing financial interest.

■ ACKNOWLEDGMENTS

This work was partially supported by the National Science Council of Taiwan, under grant no. NSC 100-2811-M-009-037. Prof. J.-Y. Juang is partially supported by the National Science Council of Taiwan and the MOE-ATP program operated at NCTU. We would like to thank Prof. Hsi-Fu Shih, Prof. Ching-Liang Dai, and Jyun-Hao Wu for sputtering (Department of Mechanical Engineering, National Chung Hsing University, Taiwan)and Dr. Yu-Hwa Shih, Dr. Shang-Jui Chiu (NTHU), and Dr. Yen-Ting Liu (NCTU) for useful discussions.

■ REFERENCES

(1) Quintana, M.; Edvinsson, T.; Hagfeldt, A.; Boschloo, G. *J. Phys. Chem. C* **2007**, *111*, 1035−1041.
(2) Greene, L. E.; Law, M.; Yuhas, B. D.; Yang, P. *J. Phys. Chem. C* **2007**, *111*, 18451−18456.
(3) Chang, Y.-K.; Hong, F. C.-N. *Nanotechnology* **2009**, *20*, 195302-1−195302-6.
(4) Meng, Q.-B.; Takahashi, K.; Zhang, X.-T.; Sutanto, I.; Rao, T. N.; Sato, O.; Fujishima, A. *Langmuir* **2003**, *19*, 3572−3574.
(5) Wu, C.-T.; Wu, J.-J. *J. Mater. Chem.* **2011**, *21*, 13605−13610.
(6) Ye, C.; Bando, Y.; Fang, X.; Shen, G.; Golberg, D. *J. Phys. Chem. C* **2007**, *111*, 12673−12676.
(7) Xu, F.; Yu, K.; Li, Q.; Zhu, Z.; Yao, T. *J. Phys. Chem. C* **2007**, *111*, 4099−4104.
(8) Song, J.; Lim, S. *J. Phys. Chem. C* **2007**, *111*, 596−600.
(9) Gao, P. X.; Ding, Y.; Wang, Z. L. *Nano Lett.* **2003**, *3*, 1315−1320.
(10) Liu, T.-Y.; Liao, H.-C.; Lin, C.-C.; Hu, S.-H.; Chen, S.-Y. *Langmuir* **2006**, *22*, 5804−5809.
(11) Zhu, K.; Wang, W.; Chen, X.; Liu, J.; Song, B.; Jiang, L.; Guo, J.; Cheng, J. *J. Alloys Compd.* **2011**, *509*, 6942−6945.
(12) Bondi, A. *Chem. Rev.* **1953**, *52*, 417−458.
(13) Chang, Y.-M.; Shieh, J.; Juang, J.-Y. *J. Phys. Chem. C* **2011**, *115*, 8983−8987.
(14) Zhang, Z.; Wang, S. J.; Yu, T.; Wu, T. *J. Phys. Chem. C* **2007**, *111*, 17500−17505.
(15) Nguyen, P.; Ng, H. T.; Meyyappan, M. *Adv. Mater.* **2005**, *17*, 1773−1777.
(16) Zhao, D.; Andreazza, C.; Andreazza, P.; Ma, J.; Liu, Y.; Shen, D. *Chem. Phys. Lett.* **2005**, *408*, 335−358.
(17) Hannon, J. B.; Kodambaka, S.; Ross, F. M.; Tromp, R. M. *Nature* **2006**, *440*, 69−71.
(18) Fan, H. J.; Lee, W.; Hauschild, R.; Alexe, M.; Rhun, G. L.; Scholz, R.; Dadgar, A.; Nielsch, K.; Kalt, H.; Krost, A.; Zacharias, M.; Gosele, U. *Small* **2006**, *2*, 561−568.
(19) Fonoberov, V. A.; Balandin, A. A. *Appl. Phys. Lett.* **2004**, *85*, 5971−5973.
(20) Fonoberov, V. A.; Balandin, A. A. *Phys. Rev. B* **2004**, *70*, 195410-1−195410-5.
(21) Fonoberov, V. A.; Alim, K. A.; Balandin, A. A.; Xiu, F.; Liu, J. *Phys. Rev. B* **2006**, *73*, 165317-1−165317-9.
(22) Fonoberov, V. A.; Balandin, A. A. *J. Nanoelectron. Optoe.* **2006**, *1*, 19−38.
(23) Alim, K. A.; Fonoberov, V. A.; Balandin, A. A. *Appl. Phys. Lett.* **2005**, *86*, 053103-1−053103-3.
(24) Greene, L. E.; Law, M.; Goldberger, J.; Kim, F.; Johnson, J. C.; Zhang, Y.; Saykally, R. J.; Yang, P. *Angew. Chem., Int. Ed.* **2003**, *42*, 3031−3034.
(25) Yu, Q.; Fu, W.; Yu, C.; Yang, H.; Wei, R.; Li, M.; Liu, S.; Sui, Y.; Liu, Z.; Yuan, M.; Zou, G. *J. Phys. Chem. C* **2007**, *111*, 17521−17526.
(26) Li, D.; Leung, Y. H.; Djurišic, A. B.; Liu, Z. T.; Xie, M. H.; Shi, S. L.; Xu, S. J.; Chan, W. K. *Appl. Phys. Lett.* **2004**, *85*, 1601−1603.
(27) Monticone, S.; Tufeu, R.; Kanaev, A. V. *J. Phys. Chem. B* **1998**, *102*, 2854−2862.
(28) Chang, Y.-M.; Jian, S.-R.; Lee, H.-Y.; Lin, C.-M.; Juang, J.-Y. *Nanotechnology* **2010**, *21*, 385705-1−385705-7.
(29) Chang, Y.-M.; Shieh, J.; Chu, P.-Y.; Lee, H.-Y.; Lin, C.-M.; Juang, J.-Y. *ACS Appl. Mater. Interfaces* **2011**, *3*, 4415−4419.
(30) Alves, H.; Pfisterer, D.; Zeuner, A.; Riemann, T.; Christen, J.; Hofmann, D. M.; Meyer, B. K. *Opt. Mater.* **2003**, *23*, 33−37.
(31) Nilsson, L.; Groening, O.; Emmenegger, C.; Kuettel, O.; Schaller, E.; Schlapbach, L.; Kind, H.; Bonard, J.-M.; Kern, K. *Appl. Phys. Lett.* **2000**, *76*, 2071−2073.
(32) Tzeng, Y.-F.; Wu, H.-C.; Sheng, P.-S.; Tai, N.-H.; Chiu, H. T.; Lee, C. Y.; Lin, I.-N. *ACS Appl. Mater. Interfaces* **2010**, *2*, 331−334.
(33) Wang, R. C.; Liu, C. P.; Huang, J. L.; Chen, S.-J.; Tseng, Y.-K.; Kung, S.-C. *Appl. Phys. Lett.* **2005**, *87*, 013110-1−013110-3.
(34) Ahsanulhaq, Q.; Kim, J.-H.; Hahn, Y.-B. *Nanotechnology* **2007**, *18*, 485307-1−485307-6.
(35) Kumar, R. T. R.; McGlynn, E.; McLoughlin, C.; Chakrabarti, S.; Smith, R. C.; Carey, J. D.; Mosnier, J. P.; Henry, M. O. *Nanotechnology* **2007**, *18*, 215704-1−215704-6.
(36) Wang, X.; Zhou, J.; Lao, C.; Song, J.; Xu, N.; Wang, Z. L. *Adv. Mater.* **2007**, *19*, 1627−1631.
(37) Chang, Y.-M.; Liu, M.-C.; Kao, P.-H.; Lin, C.-M.; Lee, H.-Y.; Juang, J.-Y. *ACS Appl. Mater. Interfaces* **2012**, in press.
(38) Li, C.; Fang, G.; Liu, N.; Li, J.; Liao, L.; Su, F.; Li, G.; Wu, X.; Hao, X. Z. *J. Phys. Chem. C* **2007**, *111*, 12566−12571.
(39) Lee, C. J.; Lee, T. J.; Lyu, S. C.; Zhang, Y.; Ruh, H.; Lee, H. J. *Appl. Phys. Lett.* **2002**, *81*, 3648−3650.
(40) Shen, X.-P.; Yuan, A.-H.; Hu, Y.-M.; Jiang, Y.; Xu, Z.; Hu, Z. *Nanotechnology* **2005**, *16*, 2039−2043.